HHS Public Access

Author manuscript

Neuroimage. Author manuscript; available in PMC 2025 December 26.

Published in final edited form as:

Neuroimage. 2025 December 01; 323: 121585. doi:10.1016/j.neuroimage.2025.121585.

Regular cannabis use modulates gamma functional connectivity with V1 during visual processing

Lauren K. Webert[a], **Nathan M. Petro**[a], **Seth D. Springer**[a,b], **Jason A. John**[a], **Lucy K. Horne**[a], **Molly E. Voller**[a], **Kyla R. De Luca**[a], **Olivia R. Carusi**[a], **Lan D. Volberding**[a], **Grant M. Garrison**[a], **Hannah J. Okelberry**[a], **Ryan Glesinger**[a], **Maggie P. Rempe**[a,b], **Tony W. Wilson**[a,b,c,*]

[a]Institute for Human Neuroscience, Boys Town National Research Hospital, 14090 Mother Teresa Ln, Boys Town, NE 68101, USA

[b]College of Medicine, University of Nebraska Medical Center, 4400 Emile Street Omaha, NE 68198, USA

[c]Department of Pharmacology and Neuroscience, Creighton University, 2500 California Plz, Omaha, NE 68178, USA

Abstract

Cannabis is a widely-used illicit substance in the United States, and heavy cannabis use has been linked to deficits across multiple cognitive domains. Mechanistically, cannabis affects endocannabinoid receptors densely distributed among GABAergic interneurons throughout the cortex and cerebellum. Such interneuronal networks are known to be crucial in the generation of fast neural gamma-band responses, which support perceptual and cognitive processing and have been frequently implicated in cannabis use. However, studies to date have tended to focus on higher-order processing supported by gamma oscillations, with limited work examining more

*Corresponding author at: Institute for Human Neuroscience, 14090 Mother Teresa Ln., Boys Town, NE 68010, USA. tony.wilson@boystown.org (T.W. Wilson).

CRediT authorship contribution statement

Lauren K. Webert: Writing – review & editing, Writing – original draft, Visualization, Validation, Software, Methodology, Formal analysis, Conceptualization. **Nathan M. Petro:** Writing – review & editing, Validation, Software, Methodology, Formal analysis, Conceptualization. **Seth D. Springer:** Writing – review & editing, Software, Methodology, Funding acquisition, Formal analysis, Data curation, Conceptualization. **Jason A. John:** Writing – review & editing, Project administration, Investigation. **Lucy K. Horne:** Writing – review & editing, Project administration, Investigation. **Molly E. Voller:** Writing – review & editing, Project administration, Investigation. **Kyla R. De Luca:** Writing – review & editing, Project administration, Investigation. **Olivia R. Carusi:** Writing – review & editing, Project administration, Investigation. **Lan D. Volberding:** Writing – review & editing, Project administration, Investigation. **Grant M. Garrison:** Writing – review & editing, Project administration, Investigation. **Hannah J. Okelberry:** Writing – review & editing, Project administration, Investigation. **Ryan Glesinger:** Writing – review & editing, Project administration, Investigation. **Maggie P. Rempe:** Writing – review & editing, Software, Formal analysis. **Tony W. Wilson:** Writing – review & editing, Validation, Supervision, Software, Resources, Project administration, Methodology, Funding acquisition, Formal analysis, Data curation, Conceptualization.

Ethical standards

The authors assert that all procedures contributing to this work comply with the ethical standards of the relevant national and institutional committees on human experimentation and with the Helsinki Declaration of 1975, as revised in 2008. The Boys Town National Research Hospital Institutional Review Board reviewed and approved this protocol. All participants gave written informed consent following a detailed description of the study.

Declaration of competing interest

All authors report no biomedical financial interests or potential conflicts of interest.

fundamental aspects of gamma circuit integrity. Herein, 84 adults who regularly use cannabis and 90 demographically-matched nonusers underwent high-density magnetoencephalography during a visual entrainment task involving three gamma-band flicker frequencies (32, 40, and 48 Hz). The resulting data were imaged in the time-frequency domain and the dynamic neural time series were extracted and tested for effects of hemisphere, frequency, and group, and then used to compute whole-brain dynamic functional connectivity. Our results indicated strong gamma entrainment in the bilateral primary visual cortices (V1), with 32 Hz responses being the strongest across both groups ($p < .001$) and right V1 activity being stronger than left across groups and frequencies ($p = .002$). Additionally, there were group-by-condition interactions in connectivity maps ($p < .005$), with the cannabis group having elevated 32 Hz connectivity between V1 and higher-order visual regions relative to controls. These findings suggest that basic gamma circuitry remains intact despite heavy cannabis use, while gamma functional connectivity is preferentially affected and this may lead to the higher-order deficits.

Keywords

Magnetoencephalography; MEG; Marijuana; Hash; Entrainment; Visual cortex

1. Introduction

Cannabis is the most commonly used illicit substance in the United States. Recently, many states have moved to legalize the use of medical and/or recreational cannabis (Bryan, 2024), with over 50% of the U.S. population now residing in states with legalized cannabis use (SAMHS, 2024). Approximately 61.8 million people reported using cannabis in 2023 alone, with 3.5 million using cannabis for the first time, and 19.2 million meeting criteria for cannabis use disorder (SAMHS, 2024). Heavy cannabis use has been linked to alterations in behavior and cognitive function. Specifically, deficits in memory, attention, and executive function have been shown in those with heavy cannabis use compared to nonusers (Ajmera et al., 2021; Andriot et al., 2022; Broyd et al., 2016; Lawn et al., 2022; Selamoglu et al., 2021). Given the broad availability and use of cannabis, further research on the mechanisms of action and impact on brain and cognitive function is critical.

Neuroimaging research has linked cannabis use to altered oscillatory activity during the execution of higher-order cognitive tasks (Castelblanco et al., 2024; McDonald et al., 2024; Rangel-Pacheco et al., 2021; Schantell et al., 2024; Springer et al., 2023b; Ward et al., 2023; Webert et al., 2025), as well as suppressed spontaneous neural activity in widespread cortical regions (Arif et al., 2021; Christopher-Hayes et al., 2021; Schantell et al., 2024, 2022; Springer et al., 2023b; Webert et al., 2025, 2024). Of note, many of these findings have involved oscillatory responses in the canonical gamma-band range (i.e., > 30 Hz; Arif et al., 2021; Castelblanco et al., 2024; Christopher-Hayes et al., 2021; Schantell et al., 2024). Such gamma oscillations are known to play a key role in many cognitive and perceptual processes (Fries, 2015; Herrmann et al., 2004; Keil et al., 1999; Muthukumaraswamy and Singh, 2013; Syed et al., 2023; Tallon-Baudry, 1999; Uhlhaas et al., 2009a, 2009b), and have been linked to the integrity of local GABAergic circuitry (Buzsáki and Wang, 2012).

This linkage between gamma oscillations and GABAergic activity may be critical to understanding the neuroimaging findings in cannabis users. Essentially, the main psychoactive component of cannabis, Δ9-tetrahydrocannabinol (THC), is known to act as an agonist of endocannabinoid 1 (CB1) receptors (Ceccarini et al., 2015), which are G-protein coupled receptors found in high concentrations on GABAergic interneurons throughout the cortex (Bloomfield et al., 2019; Lu and Mackie, 2021; Romero et al., 1997). Studies have linked their activation to alterations in synaptic transmission and plasticity (Katona et al., 1999; Puighermanal et al., 2009), leading to large-scale modifications in neuronal population dynamics. Specifically, GABAergic interneurons are among the primary generators of the gamma rhythm (Bartos et al., 2007; Buzsáki and Wang, 2012; Fries, 2015, 2009; Fries et al., 2007; Singer, 1999; Skosnik et al., 2016; Uhlhaas and Singer, 2012; Wyss et al., 2017), either via the activation of complex GABAergic inhibitory networks or the reciprocal excitatory-inhibitory loops between GABAergic interneurons and pyramidal cells (Bartos et al., 2007; Edden et al., 2009). In humans, magnetic resonance spectroscopy (MRS) studies have shown direct associations between GABA concentration levels and the strength of gamma oscillations and/or their peak frequency (Balz et al., 2016; Edden et al., 2009; Kujala et al., 2015; Muthukumaraswamy et al., 2009). Human studies have also shown that gamma power and peak frequency are tightly coupled (Proskovec et al., 2020; Spooner et al., 2018; Wilson et al., 2018).

As noted above, gamma-band oscillations across the cortex are crucial to cognitive processing and are known to be altered in adults who regularly use cannabis (Castelblanco et al., 2024; Schantell et al., 2024). These findings of altered gamma activity in regular cannabis users have generally been observed during higher-order cognitive tasks, and thus could be a reflection of network-level communication deficits involving the purported role of gamma activity in information sharing, binding, and transfer (Uhlhaas et al., 2009a; Uhlhaas and Singer, 2012). However, in higher-order tasks, many brain regions are usually active and such gamma deficits could arise from many different factors, including reduced input from lower-level cortices, volitional performance differences, or other state-based factors. Thus, whether these findings are specific to oscillatory gamma responses or more broadly reflect a basic deficit in gamma circuitry remains unknown. One method of directly probing a circuit’s capacity to generate high levels of gamma activity is through the use of entrainment paradigms. During entrainment paradigms, neuronal populations synchronize their firing to the frequency of an external stimulus (e.g., flickering light, amplitude-modulated sounds). The degree of entrainment to the stimulus is measured by the amplitude of the neural response at the frequency of the stimulus, which is thought to reflect the size of the underlying synchronized neural population (Di Russo et al., 2007; Hillyard et al., 1997; Pfurtscheller and Lopes Da Silva, 1999) and the circuit’s capacity to generate neural responses at the driving frequency. Thus, by using a driving frequency in the gamma-range, one can probe the neural circuitry underlying the generation of gamma-frequency neural activity in a tightly controlled manner, which allows for powerful inferences on the less controlled oscillatory gamma observed during higher-order tasks. Numerous studies have evaluated the integrity of auditory circuitry using gamma entrainment paradigms, usually 40 Hz auditory stimulation, and reported deficits in generating gamma neural responses in participants with autism, schizophrenia, ADHD, and many other conditions (Grent-’t-

Jong et al., 2021; Rojas et al., 2011; Wilson et al., 2012, 2008, 2007), as well as robust developmental effects (Rojas et al., 2006). Similar studies have been conducted in the visual modality using flickering light. While many of these visual studies focused more on the canonical alpha and beta frequency bands (Heinrichs-Graham et al., 2017; Heinrichs-Graham and Wilson, 2012; Herrmann, 2001; Springer et al., 2023a, 2022; Wiesman et al., 2019; Wiesman and Wilson, 2019), recent work using gamma frequency entrainment has shown robust visuocortical entrainment responses (Khachatryan et al., 2022; Petro et al., 2024).

In the current study, we assessed the integrity of visual gamma-band circuitry using a visual entrainment paradigm and magnetoencephalographic (MEG) imaging in a large sample of adults who regularly use cannabis and a demographically matched group of control nonusers. As noted above, cannabis modulates CB1 receptors located on GABAergic interneurons, which are critical for the generation of gamma-frequency neural activity. To robustly assess such gamma responses, we implemented a novel entrainment paradigm that involved a visual stimulus flickering at three distinct gamma-band frequencies (32 Hz, 40 Hz, and 48 Hz). As noted above, visual entrainment studies have historically used lower driving frequencies (i.e., alpha and beta), but recent human work has started to focus on higher frequencies such as 40 Hz visual entrainment due to its efficacy as a potential therapeutic approach for individuals with Alzheimer's disease (AD; Iaccarino et al., 2016; Jafari et al., 2020; Liu et al., 2022; Manippa et al., 2022; Menardi et al., 2022; Traikapi and Konstantinou, 2021). Further, 40 Hz has been identified as the resonant frequency of the auditory cortex through a vast body of auditory entrainment literature (Picton et al., 2003; Roß et al., 2000; Schoonhoven et al., 2003; Tang et al., 2016), although there has been less consensus on an optimal driving frequency for the visual cortex. Therefore, we chose to study 40 Hz and two additional equidistant driving frequencies (32 Hz and 48 Hz) to test if visual entrainment is stronger at slower or faster gamma-band frequencies. The experimental design was limited to three conditions to ensure task compliance and limit participant fatigue. To our knowledge, no work has utilized visual entrainment to probe gamma circuitry in the context of cannabis use, although visual entrainment in the slower beta range and auditory entrainment in gamma and beta frequencies are known to be altered (Skosnik et al., 2012, 2006). In addition to entrainment amplitude, we tested whether dynamic functional connectivity (FC) patterns differed between groups and by entrainment frequency. Our primary hypotheses were that: (1) participants in both groups would exhibit the strongest entrainment responses at 32 and 40 Hz stimulation relative to 48 Hz, based on findings in a recent normative study (Petro et al., 2024), (2) we would observe a right hemispheric bias for entrainment responses across all participants, due to previous findings of laterality differences favoring the right hemisphere in gamma entrainment (Draganova et al., 2008; Rojas et al., 2006; Ross et al., 2005; Wilson et al., 2008), and (3) that we would observe group differences in the strength of entrainment between cannabis users and nonusers, given previous literature linking regular cannabis use with reduced gamma activity (Arif et al., 2021; Castelblanco et al., 2024; Christopher-Hayes et al., 2021; Schantell et al., 2024; Webert et al., 2024). To our knowledge, no work has investigated the impact of cannabis use on visual gamma entrainment, though the auditory entrainment literature would predict reduced entrainment responses among our cannabis use group compared to nonusers

(Cortes-Briones et al., 2015; Skosnik et al., 2016, 2012). Finally, we also hypothesized that the propagation of the entrainment response from V1, as measured by FC, would be modulated by cannabis use, in agreement with previous work which has shown both reduced and increased connectivity in people who regularly use cannabis (Aloi et al., 2021; Castelblanco et al., 2024; McDonald et al., 2025; Rangel-Pacheco et al., 2021; Weyrich et al., 2023) and with the known high CB1 receptor density in regions within the visual processing network (Bloomfield et al., 2019).

2. Methods

2.1. Participants

Eighty-four individuals who regularly use cannabis (43 males, 41 females), but no other psychoactive substances, and 90 demographically-matched nonusers (47 males, 43 females) were selected for inclusion in this study from a larger cohort that also included people with HIV (PWH) and polysubstance users. All 174 adults successfully completed a visual entrainment paradigm during MEG recording, along with a battery of neuropsychological and substance use assessments (see below). As part of the inclusion criteria for the study, participants in the cannabis use group were required to have used cannabis at least twice per week for a minimum of 75% of the last 2 years. Participants were excluded from the cannabis use group if they reported using cannabis for only medicinal purposes (i.e., no recreational use), or if they had a substance use disorder other than cannabis. Exclusionary criteria for all participants in the current study included any medical illness affecting CNS function (e.g., cancer, HIV/AIDS, lupus, etc.), any neurological or psychiatric disorder (e.g., stroke, multiple sclerosis, epilepsy, Alzheimer's disease, Parkinson's disease, schizophrenia, current generalized anxiety disorder, bipolar disorder, current major depressive disorder, PTSD, autism, etc.), history of head trauma, current pregnancy, current substance use/dependence in the nonuser group, and the standard MEG/MRI exclusion criteria (i.e., ferromagnetic materials; participants must be free of excessive dental work and unremovable metal implants/jewelry). The Boys Town National Research Hospital Institutional Review Board reviewed and approved this protocol. All participants provided written informed consent following detailed description of the study.

2.2. Substance use and neuropsychological assessments

To deeply phenotype our sample, all participants underwent neuropsychological testing and those in the cannabis use group completed a battery of substance use assessments. The neuropsychological battery assessed seven cognitive domains, including learning, memory, executive function, processing speed, attention, motor dexterity, and language (Landler et al., 2024). The substance use assessments included an interview focusing on their lifetime and current (within the last 12 months) substance use history using the NIDA Quick Screen (Version 1), NIDA-Modified Alcohol, Smoking, and Substance Involvement Screening Test (ASSIST; Version 2), and Module E of the Structured Clinical Interview for the Diagnostic and Statistical Manual, 5th Edition (SCID-5). Participants also completed self-report questionnaires, including the Cannabis Use Disorders Identification Test – Revised (CUDIT-R), the Alcohol Use Disorders Identification Test (AUDIT), and a customized cannabis use questionnaire detailing their cannabis use methods and history. Participants

also provided a urine sample to confirm no substance use in the control group, and confirm cannabis use and no recent use of substances other than cannabis in the cannabis group. Nonusers were interviewed on past and current substance use using a standardized medical history interview, and alcohol use was assessed using the AUDIT.

2.3. MEG experimental paradigm

During the MEG recording, participants were seated in a nonmagnetic chair within a magnetically-shielded room and completed a 15.5-minute visual entrainment task (Fig. 1), with 246 pseudorandomized trials. For each trial, a fixation dot was centrally presented on a gray background for 2000–2500 ms, followed by the presentation of an entrainment stimulus for 1500 ms. The entrainment stimulus was a small white circle, 2.75 inches in diameter, that subtended a visual angle of 3.5° and flickered on-and-off at either 32, 40, or 48 times per second (Hz) with a 50% duty-cycle. A total of 74 trials per flicker frequency (i.e., 32 Hz, 40 Hz, and 48 Hz) and an additional 24 oddball trials were pseudorandomly presented. Participants were instructed to respond via button press with their right index finger when an oddball was detected, which consisted of the fixation dot changing from grey to blue. To ensure all participants were attending to the flickering stimuli, participants with fewer than 70% accuracy in their responses to the 24 oddball trials were excluded from all data analyses. The entrainment stimuli were presented using the Psychophysics Toolbox (Kleiner et al., 2007) and a PROPixx DLP LED projector (VPixx Technologies Inc., Saint-Bruno-de-Montarville, Canada). The stimulation frequencies were verified using a fast Fourier transform of data from a fiber-optic photodiode attached to the presentation screen while the experimental paradigm was displayed.

2.4. MEG data acquisition

MEG data acquisition, structural coregistration, preprocessing, and sensor-/source-level analyses followed a pipeline similar to a number of previous studies from our laboratory (McDonald et al., 2025; Petro et al., 2024; Schantell et al., 2024; Webert et al., 2024). All MEG recordings were conducted in a two-layer magnetically-shielded VACOSHIELD room (Vacuumschmelze, Hanau, Germany) using a 306-sensor MEGIN Truix Neo MEG system (MEGIN, Helsinki, Finland) equipped with 204 planar gradiometers and 102 magnetometers. Neuromagnetic responses were sampled continuously at 1 kHz with an acquisition bandwidth of 0.1–330 Hz. During data acquisition, participants were monitored via real-time audio-visual feeds from inside the shielded room. Each participant's MEG data were corrected for head motion and subjected to noise reduction using signal space separation with a temporal extension (Taulu and Simola, 2006). Only the gradiometer data were used in the current analyses.

2.5. Structural MRI processing, and MEG coregistration

Preceding MEG measurement, five head position indicator (HPI) coils were attached to the participant's head and localized together with three fiducial points and at least 100 scalp surface points using a 3D digitizer (Fastrak, Polhemus Navigator Sciences, Colchester, VT, USA). Once in the MEG, electrical currents at unique frequencies (e.g., 322 Hz) were fed to each of the five HPI coils, which induced measurable magnetic fields and allowed the position of each HPI coil to be accurately tracked relative to the MEG sensors throughout

the recording. Since HPI coil locations were also known in head coordinates, all MEG measurements could be transformed into a common coordinate system. With this coordinate system, participant-wise MEG data were coregistered with high-resolution structural T1-weighted MRI data prior to source reconstruction using BESA MRI (Version 3.0, BESA GmbH, Gräfelfing, Germany). Structural MRI data were transformed into standardized space and aligned parallel to the anterior and posterior commissures. Following source analysis, each participant's MEG functional images were also transformed into standardized space and spatially resampled to enable comparison across participants.

2.6. MEG preprocessing, time-frequency transformation, and sensor-level statistics

Cardiac and ocular artifacts (blinks and eye movements) were removed from the data using signal-space projection (SSP), which was accounted for during source analysis (Uusitalo and Ilmoniemi, 1997). The continuous magnetic time series was divided into 3500 ms epochs, with the baseline period being defined as the 600 ms prior to the onset of the flickering stimulus (i.e., −600 to 0 ms). Subsequently, epochs containing remaining artifacts (after cardiac and ocular artifact removal) were removed based on an individually-fixed threshold method, supplemented with visual inspection. Briefly, the amplitude and gradient distributions across all trials were determined per participant, and those trials containing the highest amplitude and/or gradient values relative to this distribution were rejected based on participant-specific thresholds. This approach was employed to minimize the impact of individual differences in sensor proximity to the brain due to overall head size and related factors, which strongly affect MEG signal amplitude. Cannabis users and nonusers did not differ in signal amplitude ($t_{167} = 0.730$, $p = 0.466$; cannabis users: $M = 1121.84$ fT/cm, $SD = 336.14$; nonusers: $M = 1173.33$ fT/cm, $SD = 541.62$) nor gradient cutoffs ($t_{167} = -0.223$, $p = 0.824$; cannabis users: $M = 257.09$ fT/(cm*ms), $SD = 134.12$; nonusers: $M = 251.50$ fT/(cm*ms), $SD = 183.78$). Further, the number of epochs retained for final analyses did not differ by condition ($F_{2,334} = 1.80$, $p = 0.167$), group ($F_{1,167} = 2.20$, $p = 0.140$), nor their interaction ($F_{2,334} = 0.449$, $p = 0.639$). Artifact-free epochs were then transformed into the time-frequency domain using complex demodulation (Kovach and Gander, 2016; Papp and Ktonas, 1977), with a resolution of 0.5 Hz and 100 ms between 2 and 100 Hz. Following time-frequency transformation, spectral power estimates per sensor were averaged across trials to generate plots of mean spectral density per sensor. These sensor-level data were then normalized using the baseline power within each 0.5 Hz frequency bin, which was calculated as the mean power during the −600 to 0 ms time period for that bin.

The time-frequency windows used for source imaging were determined by statistical analysis of the sensor-level spectrograms across the entire array of 204 gradiometers and all participants and conditions using BESA Statistics (Version 2.1, BESA GmbH, Gräfelfing, Germany). Briefly, each pixel per spectrogram was initially evaluated using a mass univariate approach based on the general linear model, followed by cluster-based permutation testing to address the problem of multiple comparisons (Ernst, 2004; Maris and Oostenveld, 2007). This two-stage procedure was utilized to minimize false positive results while maintaining sensitivity. The first stage consisted of performing paired-sample *t*-tests against baseline on each pixel per spectrogram and thresholding the output spectrograms of *t*-values at $p < 0.05$ to define time-frequency bins containing potentially significant

deviations from baseline. Time-frequency bins that survived thresholding (at $p < 0.05$) were clustered with temporally and/or spectrally neighboring bins that also survived, and cluster values were derived by summing all *t*-values within each cluster. In stage two, nonparametric permutation testing was used to derive a distribution of cluster-values and the significance level of the cluster(s) from stage one were tested directly using this permuted distribution, which was the result of 10,000 permutations. Based on this cluster-based permutation analysis, only the time-frequency windows that contained significant deviations from baseline at the $p < 0.001$, corrected, threshold across all participants were subjected to source imaging (i.e., beamforming; see results section, "MEG Sensor-Level Neural Responses," for source imaging windows).

2.7. MEG source imaging

Cortical regions were imaged through a time-frequency-resolved extension of the linearly constrained minimum variance (LCMV) beamformer (Dalal et al., 2006; Gross et al., 2001; Van Veen et al., 1997), which employs spatial filters to calculate source power for the entire brain volume. The images were derived from the cross spectral densities of all combinations of MEG gradiometers over the time-frequency range of interest, and the solution of the forward problem for each location on a grid specified by input voxel space. In principle, the beamformer operator generates a spatial filter for each grid point that passes signals without attenuation from a given neural region, while suppressing activity in all other brain areas. The filter properties arise from the forward solution (i.e., lead field matrix) for each location on a volumetric grid specified by input voxel space and from the MEG cross spectral density matrix. Basically, for each voxel, a set of beamformer weights is determined, which amounts to each MEG sensor being allocated a sensitivity weighting for activity in the particular voxel. Following convention, the source power in these images was normalized per participant using a pre-stimulus period (i.e., baseline) of equal duration and bandwidth (Hillebrand et al., 2005). Such images are typically referred to as pseudo-*t* maps, with units (pseudo-*t*) that reflect noise-normalized power differences (i.e., active vs. passive) per voxel. MEG preprocessing and imaging used the Brain Electrical Source Analysis (version 7.1) software.

2.8. Statistical analysis: neural response power

Normalized source power was computed for the selected time-frequency bands over the entire brain volume per participant at 4.0 × 4.0 × 4.0 mm resolution. Each participant's functional images were transformed into standardized space using the transform that was previously applied to the structural images and then spatially resampled. To assess the anatomical basis of the responses identified through the sensor-level analysis, the resulting 3D beamformer output maps of brain activity were averaged across all participants, entrainment frequency conditions, and time windows of interest (see below), resulting in a single grand-averaged map. Virtual sensor time series were then extracted per participant and condition from the voxels with the strongest entrainment response in the grand-averaged image in order to investigate differences in the dynamics of visual processing as a function of stimulation frequency and/or group.

To compute virtual sensors (i.e., voxel time series), we applied the sensor weighting matrix derived from the forward solution to the preprocessed signal vector, which yielded a time series for the specific voxels. For each coordinate of interest, the envelope of spectral power was computed for the frequency range used in the beamforming analysis, which was centered around each entrainment frequency (i.e., 31–33 Hz, 39–41 Hz, and 47–49 Hz; see results section, "MEG Sensor-Level Neural Responses"). From the resulting power time series, estimates of spontaneous (i.e., baseline) activity and entrainment response power were computed for each participant and spectral window (e.g., 31–33 Hz). Spontaneous power was computed from the average of the time series data across the baseline period used in the beamformer computation (i.e., −600 to −100 ms). These mean baseline values were then used to normalize the post-stimulus time-series activity, from which estimates of entrainment response power were calculated as the average across the active time windows used in the beamforming analyses (i.e., 500 to 1000 ms and 1000 to 1500 ms).

These mean entrainment neural responses were entered into a mixed-model 3 × 2 × 2 analysis of covariance (ANCOVA) with entrainment frequency (i.e., 32 Hz, 40 Hz, 48 Hz) and hemisphere (i.e., left and right) as within-subject factors, group (i.e., cannabis users and nonusers) as a between-subject factor, and AUDIT scores as a nuisance covariate. Likewise, the mean spontaneous neural activity estimates were also subjected to a mixed-model 3 × 2 × 2 ANCOVA, with entrainment frequency (i.e., 32 Hz, 40 Hz, 48 Hz) and hemisphere (i.e., left and right) as within-subject factors, group (i.e., cannabis users and nonusers) as a between-subject factor, and AUDIT as a nuisance covariate in order to test for main effects and interactions. Regarding the AUDIT, the two groups were closely matched on demographic factors, but did differ in alcohol use; thus, we included AUDIT scores as a nuisance covariate in each analysis. To reduce the impact of outliers, participants with values 3 SDs beyond their respective group means were excluded for each analysis.

2.9. Functional connectivity

To investigate how cortico-cortico interactions differed as a function of entrainment frequency and cannabis use, the peak voxel(s) in the grand-averaged whole-brain maps described above (Fig. 2; i.e., across all participants, entrainment conditions, and time windows) were used as seeds for calculation of a coherence beamformer using the dynamic imaging of coherent sources (DICS) approach (Gross et al., 2001). Briefly, this approach uses the cross-spectral densities of the voxel-wise time series data to calculate estimates of neural coherence (i.e., connectivity). These whole-brain images reflect the voxel-wise coherence of each voxel with the identified reference (seed) voxel. One whole-brain image per entrainment frequency (i.e., 32 Hz, 40 Hz, 48 Hz), time-window (i.e., 500 to 1000 ms, 1000 to 1500 ms), and participant was calculated for each cortical seed. These maps were then averaged across the two time-windows per participant, resulting in three whole-brain coherence maps (one per entrainment condition) for each seed region per participant. Because neural response strength can artificially inflate estimates of connectivity (Schoffelen and Gross, 2009), we covaried out response power from these connectivity maps. The resulting connectivity maps were examined separately per seed region using a voxel-wise mixed-effects ANCOVA, with a single three-level within-subjects factor of entrainment frequency, and a between-subjects factor of group with two levels. We again

used AUDIT scores as a covariate of no interest (see above). To account for multiple comparisons, a cluster forming threshold of $p < .005$ and cluster-extent threshold of $k \geq 15$ (i.e., at least 960 mm^3 of brain tissue) were used, based on Gaussian random fields theory (Poline et al., 1995; Worsley et al., 1996). In addition, any cluster falling within 4 cm of its seed voxel was excluded (Brookes et al., 2011). Significant clusters exhibiting group-by-entrainment condition interactions were extracted as coherence values (% change from baseline) and subjected to post-hoc *t*-tests to determine the directionality of any interactions.

4. Results

4.1. Participant demographics and substance use assessment metrics

Five participants (5 cannabis users, 0 nonusers) were excluded from the final sample due to poor attention during the task (< 70% response rate to the oddball trials). Thus, the final sample consisted of 169 participants (79 cannabis users, 90 nonusers), with comparable demographic and neuropsychological characteristics between the two groups (Table 1). Participants in each group scored within 0.5 SD of the population mean on each of the seven cognitive domains, indicating normal cognitive function. All participants completed the AUDIT and participants in the cannabis use group completed the substance use assessment battery. Independent samples *t*-tests revealed that participants in the cannabis use group had elevated total scores on the AUDIT compared to nonusers ($t_{165} = -3.99$, $p < 0.001$), but were otherwise similar on all major demographics (Table 1). Thus, AUDIT total scores were included as a nuisance covariate in all further analyses.

4.2. MEG sensor-level neural responses

Sensor-level time-frequency analyses across all participants and entrainment frequency conditions revealed significant increases in power relative to baseline in a large number of posterior sensors for each base entrainment frequency (32 Hz, 40 Hz, and 48 Hz), as well as second harmonics of the stimulation frequencies (64 Hz, 80 Hz, and 96 Hz), all of which showed increased amplitude relative to baseline ($p < .001$, corrected; Fig. 2A). These responses are consistent with a previous MEG analysis using this task (Petro et al., 2024). Given the goals of the study, we did not image the second harmonics, focusing instead on the gamma-band increases centered on each entrainment frequency in 2 Hz-wide frequency bins (i.e., 31–33 Hz, 39–41 Hz, and 47–49 Hz) using two 500 ms time windows (i.e., 500–1000 ms, and 1000–1500 ms) that captured the strongest response amplitude following the onset of the flickering stimulus (at 0 ms). Note that we imaged the 500–1000 and 1000–1500 ms windows separately due to the limited duration of our baseline period (i.e., 500 ms). Thus, we averaged across these time windows in all of our primary analyses.

4.3. Neural entrainment responses

To identify the cortical origins of the significant neural responses observed in the sensor-level time-frequency analysis, whole-brain images were computed for each entrainment condition (i.e., 32 Hz, 40 Hz, and 48 Hz) and time window (i.e., 500–1000 ms, and 1000–1500 ms), and the resulting maps were grand-averaged across all participants, entrainment

conditions, and time windows to identify peak clusters, which were found in the left and right primary visual cortices (V1; Fig. 2B).

Voxel time series data were then extracted from the peaks identified in the grand-averaged maps (i.e., left and right V1), and the mean response power per entrainment condition during the time period identified in the sensor-level analyses (i.e., 500–1500 ms) was computed. These values were then log transformed to normalize their distribution. Prior to conducting the mixed-effects ANCOVA, assumptions of normality and homogeneity of variances were assessed. A nonsignificant Shapiro-Wilk test (all ps > 0.05) and skewness and kurtosis values close to zero confirmed the normality of the distribution of the data, and Levene's test indicated that the assumption of equal variances was met (all ps > 0.05). Therefore, all key assumptions were met, and the resulting values were entered into a 3 × 2 × 2 ANCOVA, with entrainment frequency (i.e., 32 Hz, 40 Hz, 48 Hz) and hemisphere (i.e., left and right) as within-subject factors, group (i.e., cannabis users and nonusers) as a between-subject factor, and AUDIT total scores as a nuisance covariate. The ANCOVA revealed an overall effect of entrainment frequency ($F_{2,324} = 58.82$, $p < 0.001$), which was driven by stronger 32 Hz responses compared to 40 Hz ($t_{164} = 4.79$, $p < 0.001$) and 48 Hz ($t_{164} = 12.39$, $p < 0.001$), and stronger entrainment responses at 40 Hz compared to 48 Hz ($t_{164} = 12.93$, $p < 0.001$). The main effect of hemisphere was also present ($F_{1,324} = 4.19$, $p = 0.042$), whereby entrainment responses were stronger in the right V1 relative to the left V1 ($t_{164} = 2.83$, $p = 0.004$) across all entrainment frequencies. No other main effects or interactions were significant (all ps > 0.05; Fig. 3). Mauchly's test indicated that the assumption of sphericity was violated for the within-subject factor of entrainment frequency ($\chi^2(2) = 35.45$, $p < 0.001$) and the entrainment frequency-by-hemisphere interaction term ($\chi^2(2) = 12.52$, $p = 0.002$), and therefore the degrees of freedom were corrected using Greenhouse-Geisser estimates of sphericity (Entrainment frequency: $\varepsilon = 0.835$; Entrainment frequency-by-hemisphere: $\varepsilon = 0.930$), which had no effect on the results given our sample sizes.

Since this pattern of entrainment results reflected what would be expected based on the 1/f power relationship alone, we ran a follow-up rank order analysis to ascertain the percentage of participants that showed this pattern as a function of stimulation frequency (i.e., 32 > 40 > 48 Hz). It is important to note that 1/f should not have affected our entrainment estimates, as the data during the entrainment period are normalized using the baseline power in the same frequency range and expressed as percent change. Nonetheless, we felt such an analysis of peak stimulation frequency was still warranted, and the results of this are presented in Table 2. These show that less than 50% of all participants showed the pattern that would be expected based on 1/f alone, and that these percentages were virtually identical across groups.

Next, we assessed whether there were differences in spontaneous activity at each stimulation frequency during the baseline. Testing for such differences is important, as this can affect the interpretation of the stimulation-induced changes, which are expressed as a percent change from the baseline (Heinrichs-Graham et al., 2018; Heinrichs-Graham and Wilson, 2016; Wilson et al., 2014). Briefly, we computed the average spontaneous activity per condition over the baseline window for the same left and right V1 peaks from the grand-averaged

map. These values were then log transformed to normalize their distribution and entered into a mixed-effects 3 × 2 × 2 ANCOVA, with entrainment frequency and hemisphere as within-subject factors, participant group as a between-subject factor, and AUDIT total scores as a nuisance covariate. As expected, the ANCOVA revealed a significant main effect of entrainment frequency ($F_{2,324}$ = 500.18, p < 0.001), driven by stronger spontaneous 32 Hz activity compared to 40 Hz (t_{162} = 32.17, p < 0.001) and 48 Hz (t_{162} = 36.25, p < 0.001), and stronger spontaneous 40 Hz gamma compared to 48 Hz (t_{162} = 24.25, p < 0.001). Since spontaneous data reflects the non-normalized neural activity before stimulus onset in each trial, the observed conditional differences in spontaneous activity can be attributed to the 1/f power relationship. There was no significant effect of group ($F_{1,162} = 3.57 \times 10^{-5}$, p = 0.987), hemisphere ($F_{1,162}$ = 1.04, p = 0.311), nor two- or three-way interactions (all ps > 0.29), meaning that baseline gamma activity among cannabis users did not differ from that of non-using controls in any form, nor did it differ between hemispheres.

4.4. Functional connectivity

Next, we computed functional connectivity at each entrainment frequency between the visual cortical seed regions (i.e., left and right V1) and all voxels in the brain. To evaluate conditional (i.e., entrainment frequencies) and group differences, we used a voxel-wise 3 × 2 ANCOVA, including participant total scores on the AUDIT and voxel-wise source amplitude as nuisance covariates. For both the left and right V1 seeds, we observed a main effect of group and of entrainment frequency, as well as an entrainment frequency-by-group interaction effect (Fig. 4). Both interaction maps (i.e., left and right V1 as the seed regions) shared two significant clusters. One was located in the right cerebellum (p < 0.005, k > 15) and the other in the left pars opercularis (p < 0.005, k > 15). The cerebellar peaks were identical (i.e., same coordinates) in both interaction maps, whereas the left pars opercularis clusters peaked in neighboring voxels. In addition, the interaction map from the right V1 seed region revealed a third significant cluster located in the left lateral occipital cortex (p < 0.005, k > 15). Connectivity values were extracted from each significant cluster, and post-hoc testing revealed elevated connectivity in cannabis users between the right V1 and the left lateral occipital cortex at 32 Hz only (Fig. 4A; 32 Hz: t = −2.61, p = 0.010; 40 Hz: t = 0.49, p = 0.628; 48 Hz: t = 0.48, p = 0.636). Connectivity between the right cerebellum and both the left and right V1 maintained this pattern, as connectivity was stronger in cannabis users at 32 Hz only (left V1: t = −3.34, p < 0.001; right V1: t = −3.40, p < 0.001; all other ps > 0.289; Fig. 4B). Finally, cannabis users exhibited significantly elevated connectivity between the left pars opercularis and both the left V1 and right V1 at 32 Hz (left V1: t = −2.47, p = 0.015; right V1: t = −3.44, p < 0.001) and 40 Hz (Left V1: t = −3.44, p < 0.001; Right V1: t = −3.52, p < 0.001) compared to nonusers. Conversely, at 48 Hz entrainment, connectivity between the right V1 and left pars opercularis was significantly weaker in cannabis users (t = 2.40, p = 0.018), though this effect was only trending between the left V1 and left pars opercularis (t = 1.74, p = 0.084; Fig. 4C).

5. Discussion

The present study utilized MEG imaging and a visual entrainment paradigm to investigate the impact of regular cannabis use on gamma-frequency neural activity in cortical visual

areas and dynamic functional connectivity (FC) between these areas and the rest of the brain. Across all participants, we identified robust entrainment responses across the gamma spectrum in bilateral V1. Voxel time series were extracted from these peak voxels to examine the local visual processing dynamics and whole-brain functional connectivity. Our results revealed that 32 Hz elicited the strongest entrainment response, followed by 40 Hz, and finally 48 Hz stimulation in the bilateral V1 across all participants. In addition, we discovered a laterality bias such that entrainment responses were stronger in the right hemisphere compared to the left. While we did not find any effects of cannabis use in this primary visual entrainment response, the propagation of the entrainment signal to higher-order regions along the visual processing pathway differed in those who regularly use cannabis and this effect varied across the gamma frequencies. Specifically, we identified cannabis use-by-entrainment frequency interactions on FC between the right V1 and left lateral occipital cortex, bilateral V1 and the right cerebellum, and bilateral V1 and the left pars opercularis. The implications of these findings, as well as their functional relevance, are discussed below.

Our most prominent results were the cannabis group-by-entrainment frequency interaction effects on dynamic FC with the primary visual cortex, indicating that the propagation of the visual entrainment response was uniquely modulated in the cannabis use group across the gamma spectrum. Breaking apart this interaction, we found that participants in the cannabis use group consistently exhibited an increase in 32 Hz FC between the primary visual cortex and the left lateral occipital cortex, the left pars opercularis, and the right cerebellum relative to baseline, while those in the control group showed no changes from baseline in 32 Hz FC or slight decreases from baseline along these same pathways. Further, along the left pars opercularis pathway only, there were differences in 40 Hz and 48 Hz FC, such that the cannabis use group had increased FC at 40 Hz and decreased FC at 48 Hz relative to baseline, while the opposite pattern was observed in nonusers (i.e., negligible changes relative to baseline at 40 Hz and robust increases in FC at 48 Hz). Broadly, these interaction effects corroborate previous literature linking regular cannabis use to altered FC across vast cortical networks (Aloi et al., 2021; Castelblanco et al., 2024; McDonald et al., 2025; Rangel-Pacheco et al., 2021; Weyrich et al., 2023). Regarding the specific brain regions involved in the FC findings, we were not surprised given that these cortical areas are densely populated with CB1 and CB2 receptors where THC is an agonist (Bloomfield et al., 2019; Ceccarini et al., 2015). Endocannabinoid receptors are primarily located on inhibitory GABAergic interneurons, which are heavily involved in the generation of the cortical gamma rhythm (Bartos et al., 2007; Buzsáki and Wang, 2012; Fries, 2015, 2009; Fries et al., 2007; Singer, 1999; Skosnik et al., 2016; Uhlhaas and Singer, 2012; Wyss et al., 2017) and the reciprocal inhibitory-excitatory loops that underly spectral synchrony and FC throughout the cortex (Uhlhaas and Singer, 2012). One interpretation of our results builds upon this inherent mechanistic relationship between gamma oscillations and neural connectivity. Specifically, it is thought that the temporal precision of gamma activity itself plays an important role in FC by serving as a reference frame for the precise coordination of excitatory and inhibitory neuronal responses (Fries et al., 2007; Uhlhaas et al., 2009a; Uhlhaas and Singer, 2012). Disruptions to this temporal coding have been proposed to serve as a mechanism underlying many psychiatric and neurological disorders (Uhlhaas and

Singer, 2012), as evidenced by aberrant gamma-band activity and FC observed in disorders such as Alzheimer's disease (AD), schizophrenia, and autism spectrum disorder (Gonzalez-Burgos et al., 2015; Herrmann and Demiralp, 2005; Senkowski and Gallinat, 2015; Uhlhaas and Singer, 2012, 2010). An alternative but related perspective is that such temporal coding deficits are affected by changes in the excitatory/inhibitory (E/I) ratio (Rideaux et al., 2022; Sohal and Rubenstein, 2019; Yizhar et al., 2011). In this context, alterations in GABAergic signaling lead to local E/I imbalances in the circuits serving sensory processing and/or task performance, which affects the generation of gamma oscillations. Thus, our findings of aberrant FC in individuals who regularly use cannabis likely reflect alterations in neurotransmitter dynamics due to regular THC exposure, which could be due to changes in GABA directly or the net effect on the E/I ratio. Regardless, such findings are consistent with a recent MEG study, which indicated that altered behavioral performance on a task switch paradigm was distinctly related to gamma FC levels during task performance in participants who regularly use cannabis compared to controls (McDonald et al., 2025). Interestingly, this study involved FC between the visual cortex and higher-order regions similar to those observed in the current study. Thus, we speculate that our findings of aberrant FC in the context of cannabis use may underlie some of the known behavioral and cognitive deficits observed in those who regularly use cannabis (Ajmera et al., 2021; Andriot et al., 2022; Broyd et al., 2016; Lawn et al., 2022; Selamoglu et al., 2021). Although our current paradigm did not have the behavioral measures to test this claim, this is an avenue that should be further explored in future studies to provide a greater understanding of the functional impact of these aberrations.

Beyond our FC findings, we discovered that entrainment response power in V1 was sensitive to the driving frequency across all participants, such that 32 Hz entrainment was stronger than 40 and 48 Hz responses, and 40 Hz entrainment was stronger than 48 Hz. These results suggest that the visual cortices may prefer to oscillate at a resonant gamma frequency closest to 32 Hz. Of note, studies investigating auditory entrainment have consistently identified 40 Hz as the preferred frequency of the auditory cortices (Picton et al., 2003; Roß et al., 2000; Schoonhoven et al., 2003; Tang et al., 2016). While many visual entrainment studies have also reported robust entrainment at 40 Hz (Bayram et al., 2011; Herrmann, 2001; Petro et al., 2024), there remains a wide disagreement in the literature as to the exact resonant frequency of the visual cortices. For instance, EEG studies have reported stronger visual entrainment responses at lower-gamma frequencies (i.e., 32–34 Hz, 34–38 Hz) compared to higher-gamma frequencies (i.e., > 40 Hz; (Lee et al., 2021; Yoon et al., 2025), while others have reported peak responses at frequencies beyond 40 Hz (Gulbinaite et al., 2019). Additionally, many studies have found 10 Hz or 15 Hz (i.e., alpha) to elicit the strongest entrainment responses in the visual cortices (Bayram et al., 2011; Gulbinaite et al., 2019; Herrmann, 2001; Pastor et al., 2007, 2003). Despite these conflicting findings of peak responses in the alpha and gamma band, we note that, based on visual inspection, the amplitude of gamma entrainment responses tend to be much larger than the amplitude of alpha entrainment responses (Heinrichs-Graham and Wilson, 2012; Wiesman and Wilson, 2019). We further speculate that our finding of peak entrainment at 32 Hz may be due to underlying circuitry differences between the auditory and visual cortices. However, more work is needed to truly identify the ideal driving frequency of the visual cortices.

Another interesting finding was the hemispheric lateralization of the entrainment response in V1, such that entrainment was stronger in the right V1 compared to the left across all entrainment frequencies and participants. This laterality of the entrainment response has been well-documented in the auditory entrainment literature (Draganova et al., 2008; Rojas et al., 2006; Ross et al., 2005; Wilson et al., 2008), such that 40 Hz gamma power is stronger in the right auditory cortex compared to the left. To our knowledge, the visual entrainment literature has scarcely reported hemispheric lateralization of the entrainment response (Spinelli and Mecacci, 1990). However, there is a known right-hemisphere dominance during visual processing, particularly along the ventral attention network (Bartolomeo and Seidel Malkinson, 2019; Bertamini et al., 2018; Thiebaut De Schotten et al., 2011), which may underly the current findings.

Finally, it should be noted that we were surprised by the lack of group differences in the V1 entrainment response, especially given our more than adequate sample size. Due to previous findings of aberrant oscillatory responses in people who regularly use cannabis compared to controls (Castelblanco et al., 2024; McDonald et al., 2024; Rangel-Pacheco et al., 2021; Schantell et al., 2024; Springer et al., 2023b; Ward et al., 2023), we had expected to see a similar differentiation in the entrainment response between the groups. However, there are a few important distinctions to make between this literature and the current results. First, those findings were all derived from studies utilizing higher-order cognitive tasks, whereas we were probing the circuitry of a lower-level entrainment response. Secondly, the previous literature reports differences in induced oscillatory power between people who regularly use cannabis and nonuser controls, whereas we were measuring a neural entrainment response that is essentially driven by the flicker frequency of the stimulus. This is an important distinction to make, as entrainment responses reflect the phase-locking of neuronal population level activity to a driving stimulus, while induced (i.e., non-phase locked) oscillatory responses are a measure of the endogenous neural activation within a population of neurons (Duecker et al., 2021; Koelewijn et al., 2011; Lobo et al., 2021; Notbohm et al., 2016). With this in mind, a recent MEG study found no differences in evoked responses to somatosensory stimulation between regular cannabis users and nonusers (Arif et al., 2021), to which our null findings add support.

Before closing, it is important to note the limitations of the current study in order to contextualize the results. One possible limitation surrounds our task design, as we investigated a limited number of frequencies in the gamma-band, making it challenging to fully disentangle minute differences in visual cortical gamma activity between those who regularly use cannabis and nonuser controls. However, adding additional conditions would have risked decreases in task compliance and increases in participant fatigue, as at least 60 trials (following artifact rejection) are required per condition to achieve reliable beamformer reconstructions, making the task duration nearly 14 minutes with three flicker frequency conditions. Another potential limitation may arise if participants were aware of the multiple distinct flicker frequencies, as they could have paid greater attention to one over the others (i.e., had a “preferred” one). While participants were not informed about the presence of multiple flicker frequencies before the task, a questionnaire following completion of the task would have been helpful to probe participant awareness as a potential confound to our results and future studies should consider this. Another limitation of the

current study involves our participant inclusion criteria and group phenotyping, such that all participants in the cannabis use group had been using cannabis at a relatively high rate for at least the past two years. Thus, our results are not generalizable to individuals who infrequently use cannabis, nor studies of acute cannabis use. An additional limitation is that we did not investigate other measures of FC, such as phase locking, which may provide further insights into the higher-order circuitry differences we observed. Finally, while we interpret the present results using the mechanistic relationship between cannabis use, gamma activity, and GABA-mediated circuitry, future work should include measures such as GABA concentrations to confirm the mechanistic dynamics that underlie these results. Nonetheless, despite these limitations, the current study reports that the strength of gamma activity within V1 appears to be relatively normal in regular cannabis users, while the propagation of gamma activity across higher-order visual processing circuits is significantly altered in those who regularly use cannabis.

Acknowledgements

The authors thank the participants for graciously volunteering their time to participate in the study. They would also like to thank the study staff and collaborators for their contributions, and for making this study possible. This study was supported by the National Institutes of Health through grants R01-DA047828 (TWW), R01-DA056223 (TWW), R01-MH116782 (TWW), S10-OD028751 (TWW), P20-GM144641 (TWW), and F30-AG076259 (SDS).

Funding sources

R01-DA047828, R01-DA056223, R01-MH116782, S10-OD028751, P20-GM144641, and F30-AG076259.

Data availability

The data used in this article will be made publicly available at the conclusion of the study through the Collaborative Informatics and Neuroimaging Suite (COINS; https://coins.trendscenter.org/) framework.

References

Ajmera N, Collins PF, Weiss H, Luciana M, 2021. Initiation of moderately frequent cannabis use in adolescence and young adulthood is associated with declines in verbal learning and memory: a longitudinal comparison of pre- versus Post-Initiation cognitive performance. J. Int. Neuropsychol. Soc 27, 621–636. 10.1017/S1355617721000631. [PubMed: 34261549]

Aloi J, McCusker MC, Lew BJ, Schantell M, Eastman JA, Frenzel MR, Wilson TW, 2021. Altered amygdala-cortical connectivity in individuals with Cannabis use disorder. J. Psychopharmacol 35, 1365–1374. 10.1177/02698811211054163. [PubMed: 34730052]

Andriot T, Ohnmacht P, Vuilleumier P, Thorens G, Khazaal Y, Ginovart N, Ros T, 2022. Electrophysiological and behavioral correlates of cannabis use disorder. Cogn. Affect. Behav. Neurosci 22, 1421–1431. 10.3758/s13415-022-01016-w. [PubMed: 35698004]

Arif Y, Wiesman AI, Christopher-Hayes NJ, Wilson TW, 2021. Aberrant inhibitory processing in the somatosensory cortices of cannabis-users. J. Psychopharmacol 35, 1356–1364. 10.1177/02698811211050557. [PubMed: 34694190]

Balz J, Keil J, Roa Romero Y, Mekle R, Schubert F, Aydin S, Ittermann B, Gallinat J, Senkowski D, 2016. GABA concentration in superior temporal sulcus predicts gamma power and perception in the sound-induced flash illusion. NeuroImage 125, 724–730. 10.1016/j.neuroimage.2015.10.087. [PubMed: 26546865]

Bartolomeo P, Seidel Malkinson T, 2019. Hemispheric lateralization of attention processes in the human brain. Curr. Opin. Psychol 29, 90–96. 10.1016/j.copsyc.2018.12.023. [PubMed: 30711910]

Bartos M, Vida I, Jonas P, 2007. Synaptic mechanisms of synchronized gamma oscillations in inhibitory interneuron networks. Nat. Rev. Neurosci 8, 45–56. 10.1038/nrn2044. [PubMed: 17180162]

Bayram A, Bayraktaroglu Z, Karahan E, Erdogan B, Bilgic B, Ozker M, Kasikci I, Duru AD, Ademoglu A, Oztürk C, Arikan K, Tarhan N, Demiralp T, 2011. Simultaneous EEG/fMRI analysis of the resonance phenomena in steady-State visual evoked responses. Clin. EEG Neurosci 42, 98–106. 10.1177/155005941104200210. [PubMed: 21675599]

Bertamini M, Silvanto J, Norcia AM, Makin ADJ, Wagemans J, 2018. The neural basis of visual symmetry and its role in mid- and high-level visual processing. Ann. N. Y. Acad. Sci 1426, 111–126. 10.1111/nyas.13667.

Bloomfield MAP, Hindocha C, Green SF, Wall MB, Lees R, Petrilli K, Costello H, Ogunbiyi MO, Bossong MG, Freeman TP, 2019. The neuropsychopharmacology of cannabis: a review of human imaging studies. Pharmacol. Ther 195, 132–161. 10.1016/j.pharmthera.2018.10.006. [PubMed: 30347211]

Brookes MJ, Hale JR, Zumer JM, Stevenson CM, Francis ST, Barnes GR, Owen JP, Morris PG, Nagarajan SS, 2011. Measuring functional connectivity using MEG: methodology and comparison with fcMRI. NeuroImage 56, 1082–1104. 10.1016/j.neuroimage.2011.02.054. [PubMed: 21352925]

Broyd SJ, van Hell HH, Beale C, Yücel M, Solowij N, 2016. Acute and chronic effects of cannabinoids on Human cognition—a systematic review. Biol. Psychiatry 79, 557–567. 10.1016/j.biopsych.2015.12.002. [PubMed: 26858214]

Bryan K., 2024. Cannabis Overview [WWW Document]. NCSL. URL. https://www.ncsl.org/civil-and-criminal-justice/cannabis-overview#legalization (Accessed 17 February 2025).

Buzsáki G, Wang X-J, 2012. Mechanisms of gamma oscillations. Annu. Rev. Neurosci 35, 203–225. 10.1146/annurev-neuro-062111-150444. [PubMed: 22443509]

Castelblanco CA, Springer SD, Schantell M, John JA, Coutant AT, Horne LK, Glesinger R, Eastman JA, Wilson TW, 2024. Chronic cannabis users exhibit altered oscillatory dynamics and functional connectivity serving visuospatial processing. J. Psychopharmacol 38, 724–734. 10.1177/02698811241265764. [PubMed: 39087306]

Ceccarini J, Kuepper R, Kemels D, Van Os J, Henquet C, Van Laere K, 2015. [^{18} F] MK −9470 PET measurement of cannabinoid CB1 receptor availability in chronic cannabis users. Addict. Biol 20, 357–367. 10.1111/adb.12116. [PubMed: 24373053]

Christopher-Hayes NJ, Lew BJ, Wiesman AI, Schantell M, O'Neill J, May PE, Swindells S, Wilson TW, 2021. Cannabis use impacts pre-stimulus neural activity in the visual cortices of people with HIV. Hum. Brain Mapp 42, 5446–5457. 10.1002/hbm.25634. [PubMed: 34464488]

Cortes-Briones J, Skosnik PD, Mathalon D, Cahill J, Pittman B, Williams A, Sewell RA, Ranganathan M, Roach B, Ford J, D'Souza DC, 2015. Δ9-THC disrupts gamma (γ)-band neural oscillations in humans. Neuropsychopharmacology 40, 2124–2134. 10.1038/npp.2015.53. [PubMed: 25709097]

Dalal SS, Sekihara K, Nagarajan SS, 2006. Modified beamformers for coherent source region suppression. IEEE Trans. Biomed. Eng 53, 1357–1363. 10.1109/TBME.2006.873752. [PubMed: 16830939]

Di Russo F, Pitzalis S, Aprile T, Spitoni G, Patria F, Stella A, Spinelli D, Hillyard SA, 2007. Spatiotemporal analysis of the cortical sources of the steady-state visual evoked potential. Hum. Brain Mapp 28, 323–334. 10.1002/hbm.20276. [PubMed: 16779799]

Draganova R, Ross B, Wollbrink A, Pantev C, 2008. Cortical steady-State responses to Central and peripheral auditory beats. Cereb. Cortex 18, 1193–1200. 10.1093/cercor/bhm153. [PubMed: 17827173]

Duecker K, Gutteling TP, Herrmann CS, Jensen O, 2021. No evidence for entrainment: endogenous gamma oscillations and rhythmic flicker responses coexist in visual cortex. J. Neurosci 41, 6684–6698. 10.1523/JNEUROSCI.3134-20.2021. [PubMed: 34230106]

Edden RAE, Muthukumaraswamy SD, Freeman TCA, Singh KD, 2009. Orientation discrimination performance is predicted by GABA concentration and gamma oscillation frequency in human primary visual cortex. J. Neurosci 29, 15721–15726. 10.1523/JNEUROSCI.4426-09.2009. [PubMed: 20016087]

Ernst MD, 2004. Permutation methods: a basis for exact inference. Stat. Sci 19. 10.1214/088342304000000396.

Fries P., 2015. Rhythms for cognition: communication through coherence. Neuron 88, 220–235. 10.1016/j.neuron.2015.09.034. [PubMed: 26447583]

Fries P., 2009. Neuronal gamma-band synchronization as a fundamental process in cortical computation. Annu. Rev. Neurosci 32, 209–224. 10.1146/annurev.neuro.051508.135603. [PubMed: 19400723]

Fries P, Nikolíc D, Singer W, 2007. The gamma cycle. Trends Neurosci. 30, 309–316. 10.1016/j.tins.2007.05.005. [PubMed: 17555828]

Gonzalez-Burgos G, Cho RY, Lewis DA, 2015. Alterations in cortical network oscillations and parvalbumin neurons in schizophrenia. Biol. Psychiatry 77, 1031–1040. 10.1016/j.biopsych.2015.03.010. [PubMed: 25863358]

Grent-'t-Jong T, Gajwani R, Gross J, Gumley AI, Krishnadas R, Lawrie SM, Schwannauer M, Schultze-Lutter F, Uhlhaas PJ, 2021. 40-Hz auditory steady-State responses characterize circuit dysfunctions and predict clinical outcomes in clinical high-risk for psychosis participants: a magnetoencephalography study. Biol. Psychiatry 90, 419–429. 10.1016/j.biopsych.2021.03.018. [PubMed: 34116790]

Gross J, Kujala J, Hämäläinen M, Timmermann L, Schnitzler A, Salmelin R, 2001. Dynamic imaging of coherent sources: studying neural interactions in the human brain. Proc. Natl. Acad. Sci 98, 694–699. 10.1073/pnas.98.2.694. [PubMed: 11209067]

Gulbinaite R, Roozendaal DHM, VanRullen R, 2019. Attention differentially modulates the amplitude of resonance frequencies in the visual cortex. Neuroimage 203, 116146. 10.1016/j.neuroimage.2019.116146. [PubMed: 31493535]

Heinrichs-Graham E, McDermott TJ, Mills MS, Coolidge NM, Wilson TW, 2017. Transcranial direct-current stimulation modulates offline visual oscillatory activity: a magnetoencephalography study. Cortex 88, 19–31. 10.1016/j.cortex.2016.11.016. [PubMed: 28042984]

Heinrichs-Graham E, McDermott TJ, Mills MS, Wiesman AI, Wang Y-P, Stephen JM, Calhoun VD, Wilson TW, 2018. The lifespan trajectory of neural oscillatory activity in the motor system. Dev. Cogn. Neurosci 30, 159–168. 10.1016/j.dcn.2018.02.013. [PubMed: 29525417]

Heinrichs-Graham E, Wilson TW, 2016. Is an absolute level of cortical beta suppression required for proper movement? Magnetoencephalographic evidence from healthy aging. Neuroimage 134, 514–521. 10.1016/j.neuroimage.2016.04.032. [PubMed: 27090351]

Heinrichs-Graham E, Wilson TW, 2012. Presence of strong harmonics during visual entrainment: a magnetoencephalography study. Biol. Psychol 91, 59–64. 10.1016/j.biopsycho.2012.04.008. [PubMed: 22569101]

Herrmann C, Demiralp T, 2005. Human EEG gamma oscillations in neuropsychiatric disorders. Clin. Neurophysiol 116, 2719–2733. 10.1016/j.clinph.2005.07.007. [PubMed: 16253555]

Herrmann CS, 2001. Human EEG responses to 1-100 hz flicker: resonance phenomena in visual cortex and their potential correlation to cognitive phenomena. Exp. Brain Res 137, 346–353. 10.1007/s002210100682. [PubMed: 11355381]

Herrmann CS, Munk MHJ, Engel AK, 2004. Cognitive functions of gamma-band activity: memory match and utilization. Trends Cogn. Sci 8, 347–355. 10.1016/j.tics.2004.06.006. [PubMed: 15335461]

Hillebrand A, Singh KD, Holliday IE, Furlong PL, Barnes GR, 2005. A new approach to neuroimaging with magnetoencephalography. Hum. Brain Mapp 25, 199–211. 10.1002/hbm.20102. [PubMed: 15846771]

Hillyard SA, Hinrichs H, Tempelmann C, Morgan ST, Hansen JC, Scheich H, Heinze H-J, 1997. Combining steady-state visual evoked potentials and f MRI to localize brain activity during selective attention. Hum. Brain Mapp 5, 287–292. 10.1002/(SICI)1097-0193(1997)5:4<287::AID-HBM14>3.0.CO;2-B. [PubMed: 20408230]

Iaccarino HF, Singer AC, Martorell AJ, Rudenko A, Gao F, Gillingham TZ, Mathys H, Seo J, Kritskiy O, Abdurrob F, Adaikkan C, Canter RG, Rueda R, Brown EN, Boyden ES, Tsai L-H, 2016. Gamma frequency entrainment attenuates amyloid load and modifies microglia. Nature 540, 230–235. 10.1038/nature20587. [PubMed: 27929004]

Jafari Z, Kolb BE, Mohajerani MH, 2020. Neural oscillations and brain stimulation in Alzheimer's disease. Prog. Neurobiol 194, 101878. 10.1016/j.pneurobio.2020.101878. [PubMed: 32615147]

Katona I, Sperlágh B, Sík A, Käfalvi A, Vizi ES, Mackie K, Freund TF, 1999. Presynaptically located CB1 cannabinoid receptors regulate GABA release from axon terminals of specific hippocampal interneurons. J. Neurosci 19, 4544–4558. 10.1523/JNEUROSCI.19-11-04544.1999. [PubMed: 10341254]

Keil A, Müller MM, Ray WJ, Gruber T, Elbert T, 1999. Human gamma band activity and perception of a gestalt. J. Neurosci 19, 7152–7161. 10.1523/JNEUROSCI.19-16-07152.1999. [PubMed: 10436068]

Khachatryan E, Wittevrongel B, Reinartz M, Dauwe I, Carrette E, Meurs A, Van Roost D, Boon P, Van Hulle MM, 2022. Cognitive tasks propagate the neural entrainment in response to a visual 40 hz stimulation in humans. Front. Aging Neurosci 14, 1010765. 10.3389/fnagi.2022.1010765. [PubMed: 36275007]

Kleiner M, Brainard D, Pelli D, Ingling A, Murray R, Broussard C, Cornelissen, 2007. What's new in Psychtoolbox-3? Perception 36, 1–16.

Koelewijn L, Dumont JR, Muthukumaraswamy SD, Rich AN, Singh KD, 2011. Induced and evoked neural correlates of orientation selectivity in human visual cortex. Neuroimage 54, 2983–2993. 10.1016/j.neuroimage.2010.11.045. [PubMed: 21112405]

Kovach CK, Gander PE, 2016. The demodulated band transform. J. Neurosci. Methods 261, 135–154. 10.1016/j.jneumeth.2015.12.004. [PubMed: 26711370]

Kujala J, Jung J, Bouvard S, Lecaignard F, Lothe A, Bouet R, Ciumas C, Ryvlin P, Jerbi K, 2015. Gamma oscillations in V1 are correlated with GABAA receptor density: a multi-modal MEG and Flumazenil-PET study. Sci. Rep 5, 16347. 10.1038/srep16347. [PubMed: 26572733]

Landler KK, Schantell M, Glesinger R, Horne LK, Embury CM, Son JJ, Arif Y, Coutant AT, Garrison GM, McDonald KM, John JA, Okelberry HJ, Ward TW, Killanin AD, Kubat M, Furl RA, O'Neill J, Bares SH, May-Weeks PE, Becker JT, Wilson TW, 2024. People with HIV exhibit spectrally distinct patterns of rhythmic cortical activity serving cognitive flexibility. Neurobiol. Dis 201, 106680. 10.1016/j.nbd.2024.106680. [PubMed: 39326464]

Lawn W, Fernandez-Vinson N, Mokrysz C, Hogg G, Lees R, Trinci K, Petrilli K, Borissova A, Ofori S, Waters S, Michór P, Wall MB, Freeman TP, Curran HV, 2022. The CannTeen study: verbal episodic memory, spatial working memory, and response inhibition in adolescent and adult cannabis users and age-matched controls. Psychopharmacology 239, 1629–1641. 10.1007/s00213-022-06143-3. [PubMed: 35486121]

Lee K, Park Y, Suh SW, Kim S-S, Kim D-W, Lee J, Park J, Yoo S, Kim KW, 2021. Optimal flickering light stimulation for entraining gamma waves in the human brain. Sci. Rep 11, 16206. 10.1038/s41598-021-95550-1. [PubMed: 34376723]

Liu C, Han T, Xu Z, Liu J, Zhang M, Du J, Zhou Q, Duan Y, Li Y, Wang J, Cui D, Wang Y, 2022. Modulating gamma oscillations promotes brain connectivity to improve cognitive impairment. Cereb. Cortex 32, 2644–2656. 10.1093/cercor/bhab371. [PubMed: 34751749]

Lobo T, Brookes MJ, Bauer M, 2021. Can the causal role of brain oscillations be studied through rhythmic brain stimulation? J. Vis 21, 2. 10.1167/jov.21.12.2.

Lu H-C, Mackie K, 2021. Review of the endocannabinoid system. Biol. Psychiatry Cogn. Neurosci. Neuroimaging 6, 607–615. 10.1016/j.bpsc.2020.07.016. [PubMed: 32980261]

Manippa V, Palmisano A, Filardi M, Vilella D, Nitsche MA, Rivolta D, Logroscino G, 2022. An update on the use of gamma (multi)sensory stimulation for Alzheimer's disease treatment. Front. Aging Neurosci 14, 1095081. 10.3389/fnagi.2022.1095081. [PubMed: 36589536]

Maris E, Oostenveld R, 2007. Nonparametric statistical testing of EEG- and MEG-data. J. Neurosci. Methods 164, 177–190. 10.1016/j.jneumeth.2007.03.024. [PubMed: 17517438]

McDonald KM, Schantell M, Horne LK, John JA, Rempe MP, Glesinger R, Okelberry HJ, Coutant AT, Springer SD, Mansouri A, Embury CM, Arif Y, Wilson TW, 2024. The neural oscillations serving task switching are altered in cannabis users. J. Psychopharmacol 38, 471–480. 10.1177/02698811241235204. [PubMed: 38418434]

McDonald KM, Schantell M, John JA, Coutant AT, Glesinger R, Horne LK, Okelberry HJ, Springer SD, Embury CM, Arif Y, Wilson TW, 2025. Altered functional connectivity dynamics serving

cognitive flexibility in regular cannabis users. Addict. Biol 30, e70023. 10.1111/adb.70023. [PubMed: 40042248]

Menardi A, Rossi S, Koch G, Hampel H, Vergallo A, Nitsche MA, Stern Y, Borroni B, Cappa SF, Cotelli M, Ruffini G, El-Fakhri G, Rossini PM, Dickerson B, Antal A, Babiloni C, Lefaucheur J-P, Dubois B, Deco G, Ziemann U, Pascual-Leone A, Santarnecchi E, 2022. Toward noninvasive brain stimulation 2.0 in Alzheimer's disease. Ageing Res. Rev 75, 101555. 10.1016/j.arr.2021.101555. [PubMed: 34973457]

Muthukumaraswamy SD, Edden RAE, Jones DK, Swettenham JB, Singh KD, 2009. Resting GABA concentration predicts peak gamma frequency and fMRI amplitude in response to visual stimulation in humans. Proc. Natl. Acad. Sci 106, 8356–8361. 10.1073/pnas.0900728106. [PubMed: 19416820]

Muthukumaraswamy SD, Singh KD, 2013. Visual gamma oscillations: the effects of stimulus type, visual field coverage and stimulus motion on MEG and EEG recordings. NeuroImage 69, 223–230. 10.1016/j.neuroimage.2012.12.038. [PubMed: 23274186]

Notbohm A, Kurths J, Herrmann CS, 2016. Modification of brain oscillations via rhythmic light stimulation provides evidence for entrainment but not for superposition of event-related responses. Front. Hum. Neurosci 10. 10.3389/fnhum.2016.00010.

Papp N, Ktonas P, 1977. Critical evaluation of complex demodulation techniques for the quantification of bioelectrical activity. Biomed. Sci. Instrum 13, 135–145. [PubMed: 871500]

Pastor M, Valencia M, Artieda J, Alegre M, Masdeu J, 2007. Topography of cortical activation differs for fundamental and harmonic frequencies of the steady-State visual-evoked responses. An EEG and PET H215O study. Cereb. Cortex 17, 1899–1905. 10.1093/cercor/bhl098. [PubMed: 17060366]

Pastor MA, Artieda J, Arbizu J, Valencia M, Masdeu JC, 2003. Human cerebral activation during steady-State visual-evoked responses. J. Neurosci 23, 11621–11627. 10.1523/JNEUROSCI.23-37-11621.2003. [PubMed: 14684864]

Petro NM, Webert LK, Springer SD, Okelberry HJ, John JA, Horne LK, Glesinger R, Rempe MP, Wilson TW, 2024. Optimal gamma-band entrainment of visual cortex. Hum. Brain Mapp 45, e26775. 10.1002/hbm.26775. [PubMed: 38970249]

Pfurtscheller G, Lopes Da Silva FH, 1999. Event-related EEG/MEG synchronization and desynchronization: basic principles. Clin. Neurophysiol 110, 1842–1857. 10.1016/S1388-2457(99)00141-8. [PubMed: 10576479]

Picton TW, John MS, Dimitrijevic A, Purcell D, 2003. Human auditory steady-state responses. Int. J. Audiol 42, 177–219. 10.3109/14992020309101316. [PubMed: 12790346]

Poline J-B, Worsley KJ, Holmes AP, Frackowiak RSJ, Friston KJ, 1995. Estimating smoothness in statistical parametric maps: variability of p values. J. Comput. Assist. Tomogr 19, 788–796. 10.1097/00004728-199509000-00017. [PubMed: 7560327]

Proskovec AL, Spooner RK, Wiesman AI, Wilson TW, 2020. Local cortical thickness predicts somatosensory gamma oscillations and sensory gating: a multimodal approach. NeuroImage 214, 116749. 10.1016/j.neuroimage.2020.116749. [PubMed: 32199953]

Puighermanal E, Marsicano G, Busquets-Garcia A, Lutz B, Maldonado R, Ozaita A, 2009. Cannabinoid modulation of hippocampal long-term memory is mediated by mTOR signaling. Nat. Neurosci 12, 1152–1158. 10.1038/nn.2369. [PubMed: 19648913]

Rangel-Pacheco A, Lew BJ, Schantell MD, Frenzel MR, Eastman JA, Wiesman AI, Wilson TW, 2021. Altered Fronto-occipital connectivity during visual selective attention in regular cannabis users. Psychopharmacology 238, 1351–1361. 10.1007/s00213-020-05717-3. [PubMed: 33241479]

Rideaux R, Ehrhardt SE, Wards Y, Filmer HL, Jin J, Deelchand DK, Marjańska M, Mattingley JB, Dux PE, 2022. On the relationship between GABA + and glutamate across the brain. NeuroImage 257, 119273. 10.1016/j.neuroimage.2022.119273. [PubMed: 35526748]

Rojas D, Maharajh K, Teale P, Kleman M, Benkers T, Carlson J, Reite M, 2006. Development of the 40Hz steady state auditory evoked magnetic field from ages 5 to 52. Clin. Neurophysiol 117, 110–117. 10.1016/j.clinph.2005.08.032. [PubMed: 16316780]

Rojas DC, Teale PD, Maharajh K, Kronberg E, Youngpeter K, Wilson LB, Wallace A, Hepburn S, 2011. Transient and steady-state auditory gamma-band responses in first-degree relatives of people with autism spectrum disorder. Mol. Autism 2, 11. 10.1186/2040-2392-2-11. [PubMed: 21729257]

Romero J, de Miguel R, Ramos JA, Fernández-Ruiz JJ, 1997. The activation of cannabinoid receptors in striatonigral gabaergic neurons inhibited Gaba uptake. Life Sci 62, 351–363. 10.1016/S0024-3205(97)01117-X.

Roß B, Borgmann C, Draganova R, Roberts LE, Pantev C, 2000. A high-precision magnetoencephalographic study of human auditory steady-state responses to amplitude-modulated tones. J. Acoust. Soc. Am 108, 679–691. 10.1121/1.429600. [PubMed: 10955634]

Ross B, Herdman AT, Pantev C, 2005. Right hemispheric laterality of Human 40 hz auditory steady-state responses. Cereb. Cortex 15, 2029–2039. 10.1093/cercor/bhi078. [PubMed: 15772375]

SAMHS, 2024. Key Substance Use and Mental Health Indicators in the United States: Results from the 2023 National Survey on Drug Use and Health. HHS Publ. No PEP24-07-021 NSDUH Ser. H-59.

Schantell M, John JA, Coutant AT, Okelberry HJ, Horne LK, Glesinger R, Springer SD, Mansouri A, May-Weeks PE, Wilson TW, 2024. Chronic cannabis use alters the spontaneous and oscillatory gamma dynamics serving cognitive control. Hum. Brain Mapp 45, e26787. 10.1002/hbm.26787. [PubMed: 39023178]

Schantell M, Springer SD, Arif Y, Sandal ME, Willett MP, Johnson HJ, Okelberry HJ, O'Neill JL, May PE, Bares SH, Wilson TW, 2022. Regular cannabis use modulates the impact of HIV on the neural dynamics serving cognitive control. J. Psychopharmacol 36, 1324–1337. 10.1177/02698811221138934. [PubMed: 36416285]

Schoffelen J, Gross J, 2009. Source connectivity analysis with MEG and EEG. Hum. Brain Mapp 30, 1857–1865. 10.1002/hbm.20745. [PubMed: 19235884]

Schoonhoven R, Boden CJR, Verbunt JPA, De Munck JC, 2003. A whole head MEG study of the amplitude-modulation-following response: phase coherence, group delay and dipole source analysis. Clin. Neurophysiol 114, 2096–2106. 10.1016/S1388-2457(03)00200-1. [PubMed: 14580607]

Selamoglu A, Langley C, Crean R, Savulich G, Cormack F, Sahakian BJ, Mason B, 2021. Neuropsychological performance in young adults with cannabis use disorder. J. Psychopharmacol 35, 1349–1355. 10.1177/02698811211050548. [PubMed: 34694178]

Senkowski D, Gallinat J, 2015. Dysfunctional prefrontal gamma-band oscillations reflect working memory and other cognitive deficits in schizophrenia. Biol. Psychiatry 77, 1010–1019. 10.1016/j.biopsych.2015.02.034. [PubMed: 25847179]

Singer W., 1999. Neuronal synchrony: a versatile code for the definition of relations? Neuron 24, 49–65. 10.1016/S0896-6273(00)80821-1. [PubMed: 10677026]

Skosnik PD, Cortes-Briones JA, Hajós M, 2016. It's all in the rhythm: the role of cannabinoids in neural oscillations and psychosis. Biol. Psychiatry 79, 568–577. 10.1016/j.biopsych.2015.12.011. [PubMed: 26850792]

Skosnik PD, D'Souza DC, Steinmetz AB, Edwards CR, Vollmer JM, Hetrick WP, O'Donnell BF, 2012. The effect of chronic cannabinoids on broadband EEG neural oscillations in humans. Neuropsychopharmacology 37, 2184–2193. 10.1038/npp.2012.65. [PubMed: 22713908]

Skosnik PD, Krishnan G, Vohs J, Odonnell B, 2006. The effect of cannabis use and gender on the visual steady state evoked potential. Clin. Neurophysiol 117, 144–156. 10.1016/j.clinph.2005.09.024. [PubMed: 16364685]

Sohal VS, Rubenstein JLR, 2019. Excitation-inhibition balance as a framework for investigating mechanisms in neuropsychiatric disorders. Mol. Psychiatry 24, 1248–1257. 10.1038/s41380-019-0426-0. [PubMed: 31089192]

Spinelli D, Mecacci L, 1990. Handedness and hemispheric asymmetry of pattern reversal visual-evoked potentials. Brain Cogn. 13, 193–210. 10.1016/0278-2626(90)90050-X. [PubMed: 2390234]

Spooner RK, Wiesman AI, Mills MS, O'Neill J, Robertson KR, Fox HS, Swindells S, Wilson TW, 2018. Aberrant oscillatory dynamics during somatosensory processing in HIV-infected adults. Neuroimage Clin. 20, 85–91. 10.1016/j.nicl.2018.07.009. [PubMed: 30094159]

Springer SD, Erker TD, Schantell M, Johnson HJ, Willett MP, Okelberry HJ, Rempe MP, Wilson TW, 2023a. Disturbances in primary visual processing as a function of healthy aging. Neuroimage 271, 120020. 10.1016/j.neuroimage.2023.120020. [PubMed: 36914104]

Springer SD, Spooner RK, Schantell M, Arif Y, Frenzel MR, Eastman JA, Wilson TW, 2023b. Regular recreational Cannabis users exhibit altered neural oscillatory dynamics during attention reorientation. Psychol. Med 53, 1205–1214. 10.1017/S0033291721002671. [PubMed: 34889178]

Springer SD, Wiesman AI, May PE, Schantell M, Johnson HJ, Willett MP, Castelblanco CA, Eastman JA, Christopher-Hayes NJ, Wolfson SL, Johnson CM, Murman DL, Wilson TW, 2022. Altered visual entrainment in patients with Alzheimer's disease: magnetoencephalography evidence. Brain Commun. 4, fcac198. 10.1093/braincomms/fcac198. [PubMed: 35974799]

Syed SA, Schnakenberg Martin AM, Cortes-Briones JA, Skosnik PD, 2023. The relationship between cannabinoids and neural oscillations: how cannabis disrupts sensation, perception, and cognition. Clin. EEG Neurosci 54, 359–369. 10.1177/15500594221138280. [PubMed: 36426543]

Tallon-Baudry C, 1999. Oscillatory gamma activity in humans and its role in object representation. Trends Cogn. Sci 3, 151–162. 10.1016/S1364-6613(99)01299-1. [PubMed: 10322469]

Tang H, Crain S, Johnson BW, 2016. Dual temporal encoding mechanisms in human auditory cortex: evidence from MEG and EEG. Neuroimage 128, 32–43. 10.1016/j.neuroimage.2015.12.053. [PubMed: 26763154]

Taulu S, Simola J, 2006. Spatiotemporal signal space separation method for rejecting nearby interference in MEG measurements. Phys. Med. Biol 51, 1759–1768. 10.1088/0031-9155/51/7/008. [PubMed: 16552102]

Thiebaut De Schotten M, Dell'Acqua F, Forkel S, Simmons A, Vergani F, Murphy DGM, Catani M, 2011. A lateralized brain network for visuo-spatial attention. Nat. Preced 10.1038/npre.2011.5549.1.

Traikapi A, Konstantinou N, 2021. Gamma oscillations in Alzheimer's disease and their potential therapeutic role. Front. Syst. Neurosci 15, 782399. 10.3389/fnsys.2021.782399. [PubMed: 34966263]

Uhlhaas PJ, Pipa G, Lima B, Melloni L, Neuenschwander S, Nikolíc D, Singer W, 2009a. Neural synchrony in cortical networks: history, concept and current status. Front. Integr. Neurosci 3.

Uhlhaas PJ, Roux F, Singer W, Haenschel C, Sireteanu R, Rodriguez E, 2009b. The development of neural synchrony reflects late maturation and restructuring of functional networks in humans. Proc. Natl. Acad. Sci 106, 9866–9871. 10.1073/pnas.0900390106. [PubMed: 19478071]

Uhlhaas PJ, Singer W, 2012. Neuronal dynamics and neuropsychiatric disorders: toward a translational paradigm for dysfunctional large-scale networks. Neuron 75, 963–980. 10.1016/j.neuron.2012.09.004. [PubMed: 22998866]

Uhlhaas PJ, Singer W, 2010. Abnormal neural oscillations and synchrony in schizophrenia. Nat. Rev. Neurosci 11, 100–113. 10.1038/nrn2774. [PubMed: 20087360]

Uusitalo MA, Ilmoniemi RJ, 1997. Signal-space projection method for separating MEG or EEG into components. Med. Biol. Eng. Comput 35, 135–140. 10.1007/BF02534144. [PubMed: 9136207]

Van Veen BD, Van Drongelen W, Yuchtman M, Suzuki A, 1997. Localization of brain electrical activity via linearly constrained minimum variance spatial filtering. IEEE Trans. Biomed. Eng 44, 867–880. 10.1109/10.623056. [PubMed: 9282479]

Ward TW, Springer SD, Schantell M, John JA, Horne LK, Coutant AT, Okelberry HJ, Willett MP, Johnson HJ, Killanin AD, Heinrichs-Graham E, Wilson TW, 2023. Regular cannabis use alters the neural dynamics serving complex motor control. Hum. Brain Mapp 44, 6511–6522. 10.1002/hbm.26527. [PubMed: 37955378]

Webert LK, Schantell M, Horne LK, John JA, Glesinger R, O'Neill J, Kubat M, Coutant AT, Ende GC, Bares SH, May-Weeks PE, Wilson TW, 2025. Motor-related neural dynamics are modulated by regular cannabis use among people with HIV. J. Neuroimmune Pharmacol 20, 63. 10.1007/s11481-025-10219-0. [PubMed: 40473990]

Webert LK, Schantell M, John JA, Coutant AT, Okelberry HJ, Horne LK, Sandal ME, Mansouri A, Wilson TW, 2024. Regular cannabis use modulates gamma activity in brain regions serving motor control. J. Psychopharmacol, 02698811241268876 10.1177/02698811241268876.

Weyrich L, Arif Y, Schantell M, Johnson HJ, Willett MP, Okelberry HJ, Wilson TW, 2023. Altered functional connectivity and oscillatory dynamics in polysubstance and cannabis only users during visuospatial processing. Psychopharmacology 240, 769–783. 10.1007/s00213-023-06318-6. [PubMed: 36752815]

Wiesman AI, Groff BR, Wilson TW, 2019. Frontoparietal networks mediate the behavioral impact of alpha inhibition in visual cortex. Cereb. Cortex N. Y. N 29, 3505–3513. 10.1093/cercor/bhy220, 1991.

Wiesman AI, Wilson TW, 2019. Alpha frequency entrainment reduces the effect of visual distractors. J. Cogn. Neurosci 31, 1392–1403. 10.1162/jocn_a_01422. [PubMed: 31059352]

Wilson TW, Heinrichs-Graham E, Becker KM, 2014. Circadian modulation of motor-related beta oscillatory responses. Neuroimage 102, 531–539. 10.1016/j.neuroimage.2014.08.013. [PubMed: 25128712]

Wilson TW, Hernandez OO, Asherin RM, Teale PD, Reite ML, Rojas DC, 2008. Cortical gamma generators suggest abnormal auditory circuitry in early-onset psychosis. Cereb. Cortex 18, 371–378. 10.1093/cercor/bhm062. [PubMed: 17557901]

Wilson TW, McDermott TJ, Mills MS, Coolidge NM, Heinrichs-Graham E, 2018. tDCS modulates visual gamma oscillations and basal alpha activity in occipital cortices: evidence from MEG. Cereb. Cortex 28, 1597–1609. 10.1093/cercor/bhx055. [PubMed: 28334214]

Wilson TW, Rojas DC, Reite ML, Teale PD, Rogers SJ, 2007. Children and adolescents with autism exhibit reduced MEG steady-state gamma responses. Biol. Psychiatry 62, 192–197. 10.1016/j.biopsych.2006.07.002. [PubMed: 16950225]

Wilson TW, Wetzel MW, White ML, Knott NL, 2012. Gamma-frequency neuronal activity is diminished in adults with attention-deficit/hyperactivity disorder: a pharmaco-MEG study. J. Psychopharmacol. Oxf. Engl 26, 771–777. 10.1177/0269881111430731.

Worsley KJ, Marrett S, Neelin P, Vandal AC, Friston KJ, Evans AC, 1996. A unified statistical approach for determining significant signals in images of cerebral activation. Hum. Brain Mapp 4, 58–73. 10.1002/(SICI)1097-0193(1996)4:1<58::AID-HBM4>3.0.CO;2-O. [PubMed: 20408186]

Wyss C, Tse DHY, Kometer M, Dammers J, Achermann R, Shah NJ, Kawohl W, Neuner I, 2017. GABA metabolism and its role in gamma-band oscillatory activity during auditory processing: an MRS and EEG study: GABA and its role in high-frequency EEG oscillations. Hum. Brain Mapp 38, 3975–3987. 10.1002/hbm.23642. [PubMed: 28480987]

Yizhar O, Fenno LE, Prigge M, Schneider F, Davidson TJ, O'Shea DJ, Sohal VS, Goshen I, Finkelstein J, Paz JT, Stehfest K, Fudim R, Ramakrishnan C, Huguenard JR, Hegemann P, Deisseroth K, 2011. Neocortical excitation/inhibition balance in information processing and social dysfunction. Nature 477, 171–178. 10.1038/nature10360. [PubMed: 21796121]

Yoon E, Park Y, Kim HJ, Park J, Han JW, Woo SJ, Yoo S, Kim KW, 2025. Center frequency as optimal frequency of visual stimulation for spreading entrained gamma rhythms to other target brain regions in cognitively normal older adults. GeroScience. 10.1007/s11357-025-01552-6.

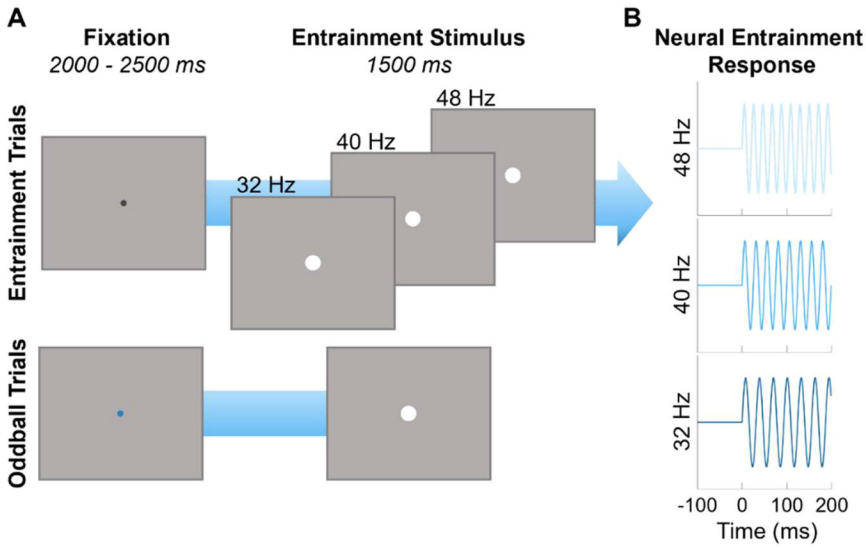

Fig. 1.

Entrainment task design. (A) Participants completed 246 trials of a visual entrainment paradigm, consisting of 222 entrainment trials (i.e., 74 trials per entrainment frequency) and 24 oddball trials. Each trial began with a fixation dot presented for an average of 2250 ms (variable ISI: 2000–2500 ms), followed by an entrainment stimulus period lasting 1500 ms. The trial type (i.e., entrainment trial or oddball trial) was determined by the fixation dot color being black or blue, respectively. During oddball trials, participants were instructed to respond to the blue fixation dot with a button press using their index finger; these trials were utilized to confirm the participant was actively attending to the entrainment stimuli throughout the task and were excluded from further analyses. During entrainment trials, the entrainment stimulus consisted of a white dot presented on a gray background, flickering on-and-off at either 32 Hz, 40 Hz, or 48 Hz. (B) Sine waves illustrating the entrainment patterns for each of the three entrainment stimulus frequencies.

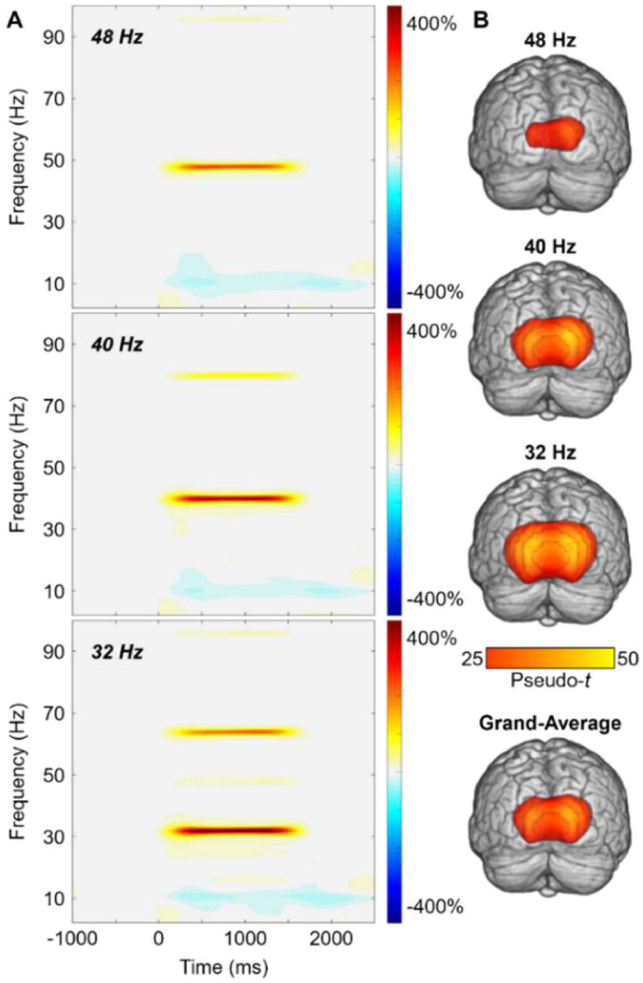

Fig. 2.

Sensor- and source-level activity during visual entrainment. (A) Averaged time-frequency spectrograms across all participants from a posterior sensor (MEG2112) for 48 Hz (top), 40 Hz (middle), and 32 Hz (bottom) entrainment conditions. Time (ms) is shown on the *x*-axis and frequency (Hz) on the *y*-axis. The color scale bar to the right illustrates the percent change in power relative to the baseline period (−600 to 0 ms). Clear entrainment can be seen at each fundamental entrainment frequency and at the 2nd harmonic, especially for the 32 and 40 Hz conditions. (B) Mean beamformer images (pseudo-*t*; see color scale bar) of the entrainment frequency for (from top to bottom) the 48, 40, and 32 Hz conditions, as well as the grand-average of all three entrainment conditions. The functional images show that visual entrainment responses consistently peaked in primary visual cortices (V1) for each stimulation frequency.

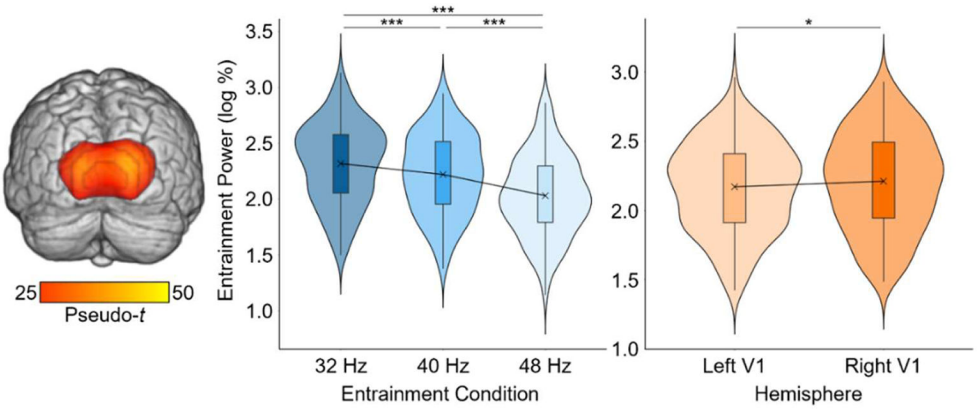

Fig. 3.

Hemispheric and frequency effects on entrainment power. (Left): The brain map depicts the average entrainment response across all three entrainment conditions, both time windows, and all participants (i.e., the grand average). (Middle): Box plots illustrating the entrainment response from 500 to 1500 ms, which were extracted from bilateral primary visual peaks (V1) at each entrainment frequency and averaged across hemispheres. The X denotes the mean per condition, the box edges are the first and third quartiles, and the whiskers indicate the minima and maxima. The surrounding violin plots illustrate the probability density. A 3 × 2 × 2 ANCOVA revealed that the entrainment response was strongest for 32 Hz, followed by 40 Hz, and weakest for 48 Hz entrainment frequencies ($F_{2,324} = 58.82$, $p < 0.001$), across both hemispheres and groups. (Right): The entrainment response, averaged across groups and entrainment frequency conditions, was also stronger in the right V1 compared to the left V1 ($F_{2,324} = 4.19$, $p = 0.042$). *$p \leq 0.05$; ***$p \leq 0.001$.

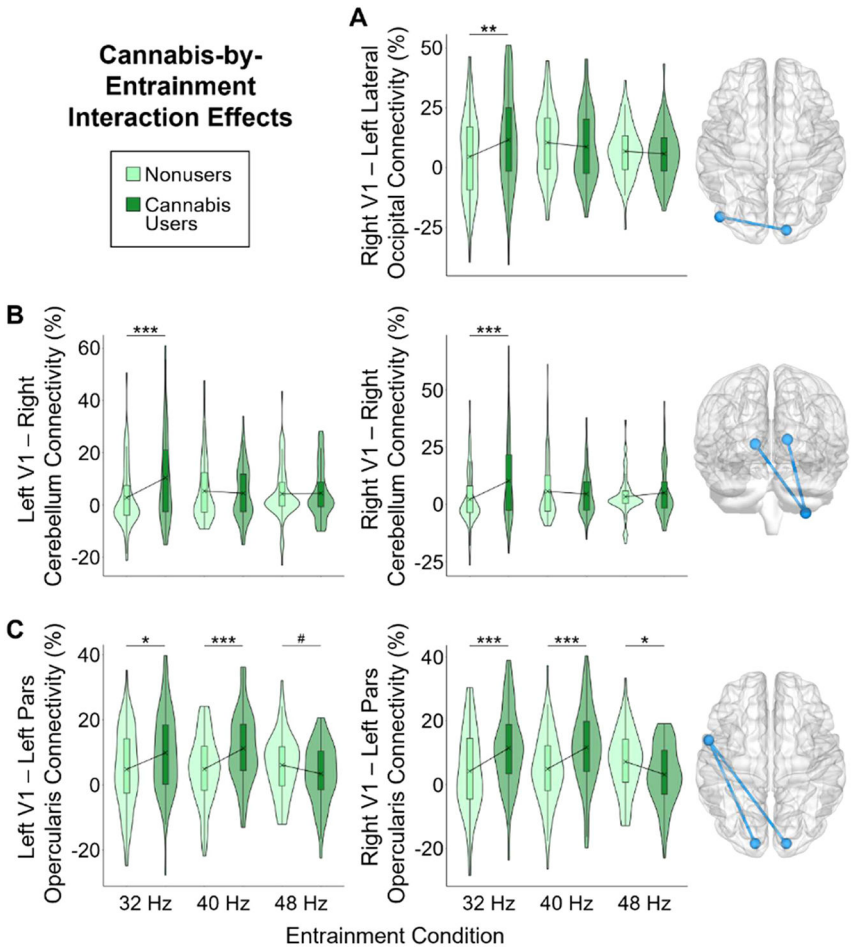

Fig. 4.

Cannabis use by entrainment frequency interaction in functional connectivity with the primary visual cortices. The box plots illustrate the strength of connectivity (%) for each entrainment condition per group. The X denotes the mean, the box edges are the first and third quartiles, and the whiskers indicate the minima and maxima. The surrounding violin plots illustrate the probability density. The brain maps on the right depict the corresponding brain regions. Voxel-wise 3 × 2 ANCOVAs on connectivity values from the left and right primary visual (V1) seed regions revealed significant interactions between cannabis use and entrainment frequency in (A) the left lateral occipital cortex (right V1 seed only), (B) the right cerebellum, and (C) the left pars opercularis. Follow-up testing revealed that overall, cannabis users exhibited elevated connectivity between the right V1 and the left lateral occipital cortex and between the bilateral V1 and the right cerebellum at 32 Hz entrainment only, as well as elevated connectivity between the bilateral V1 and the left pars opercularis at 32 and 40 Hz entrainment frequencies compared to nonusers. The opposite pattern was observed between bilateral V1 and the left pars opercularis at 48 Hz (i.e., stronger connectivity in nonuser controls). $^{\#}p \leq 0.10$; $^{*}p \leq 0.05$; $^{**}p \leq 0.01$; $^{***}p \leq 0.001$.

Table 1

Participant characteristics.

	Nonusers ***n*** **= 90**	**Users** ***n*** **= 79**	**Total** ***n*** **= 169**	***p*-value**
Age (years)	19–57; 37.04 (11.52)	20–66; 37.22 (10.50)	19–66; 37.12 (11.02)	0.915
Sex (Male/Female)	47/43	40/39	87/82	0.838
Race (White/BAA/Other/Not Reported)	68/9/13/0	65/8/4/2	133/17/17/2	0.159
Ethnicity (HL/Not HL/Not Reported)	7/82/1	9/70/0	16/152/1	0.475
Learning Domain	51.05 (7.09)	46.98 (8.51)	49.14 (8.03)	-
Memory Domain	49.47 (7.22)	47.89 (7.54)	48.74 (7.39)	-
Attention Domain	54.09 (9.45)	52.21 (8.43)	53.21 (9.01)	-
Processing Speed Domain	50.66 (7.56)	49.10 (7.90)	49.93 (7.73)	-
Executive Function Domain	55.63 (7.78)	54.14 (7.59)	54.93 (7.71)	-
Language Domain	47.85 (9.21)	50.48 (8.42)	49.08 (8.92)	-
Motor Dexterity Domain	50.72 (9.14)	51.15 (10.41)	50.92 (9.73)	-
AUDIT Total Score	0–13; 2.89 (2.48)	0–19; 5.13 (4.57)	0–19; 3.95 (3.78)	< 0.001
Age of First Use (years)	-	5–27; 15.69 (3.15)	-	-
Age of Daily Use (years)	-	13–50; 21.27 (7.38)	-	-
Estimated Number of Lifetime Uses	-	6389.34 (3915.90)	-	-

Notes. Means and SDs are displayed for all variables except sex, race, and ethnicity, which are displayed as the number of participants in each respective category. BAA – Black or African American; Other - Pacific Islander, American Indian/Alaska Native, and more than one race; HL – Hispanic or Latino; AUDIT – Alcohol Use Disorders Identification Test.

Table 2

Peak entrainment response and rank order.

Peak and Rank Order	Nonusers *n* = 90	Users *n* = 79	Total *n* = 169
32 Hz Peak	**57 (63.33%)**	**48 (60.76%)**	**105 (62.13%)**
32–40–48 Hz	45 (50.00%)	38 (48.10%)	83 (49.11%)
32–40–48 Hz	12 (13.33%)	10 (12.66%)	22 (13.02%)
40 Hz Peak	**29 (32.22%)**	**27 (34.18%)**	**56 (33.14%)**
40–31–48 Hz	20 (22.22%)	19 (24.05%)	39 (23.08%)
40–48–32 Hz	9 (10.00%)	8 (10.13%)	17 (10.06%)
48 Hz Peak	**4 (4.44%)**	**4 (5.06%)**	**8 (4.73%)**
48–40–32 Hz	3 (3.33%)	3 (3.80%)	6 (3.55%)
48–32–40 Hz	1 (1.11%)	1 (1.27%)	2 (1.18%)

Notes. The number of participants are shown for each peak entrainment frequency category, and are further broken down by rank order.